Leaf-based extracts of Nepal origin plants as efficient inhibitors for controlling rebar corrosion in concrete pore solution

M. Gautam, N.P. Bhattarai* and J. Bhattarai**

Central Department of Chemistry, Tribhuvan University, Kirtipur 44618, Kathmandu, Nepal

*E-mail: *bhattarai_05@yahoo.com; **neutan08@gmail.com*

Abstract

Reinforced concrete foundation (RCF) faces the challenges of early reinforcement concrete corrosion. Understanding such concrete corrosion mechanisms and developing effective mitigation strategies is crucial to ensure the durability of the RCF. The study aimed to investigate the effectiveness of leaf extracts from *Ziziphus budhensis* (LEZB) and *Tagetes erecta* (LETE) as eco-friendly corrosion inhibitors in a saturated $Ca(OH)_2$ solution with a pH of around 11.5, considered as SCP (simulated concrete pore) solution. The weight loss (WL) experiment lasted over four months to assess the ability of these leaf-based extracts to inhibit corrosion of mild steel rod (MiSR) in SCP solutions with 500 ppm, 1000 ppm, 2000 ppm, 4000 ppm LEZB and LETE at laboratory temperature (*i.e.*, 25°C). The highest corrosion inhibiting efficiency percentage reached at 4000 ppm LEZB, with 91.22% and 81.48% efficacy measured by gravimetric and electrochemical (EC) methods, respectively. Corrosion current density decreases with increasing LEZB or LETE concentrations in the SCP, as revealed by the EC study. Both extracts contain phyto-molecules (polyphenols, alkaloids, and flavonoids), which adhere to the surface of MiSR in SCP solution, thus impeding cathodic, anodic, or both reactions. In addition to WL and EC analyses, we used scanning electron microscopy with energy dispersive X-ray (SEM/EDX) and white light interferometry (WLI) techniques to study changes in the surface morphology of a passive corrosion barrier film formed on MiSR surface after being immersed for approximately four months in SCP solution without and with LEZB or LETE.

Received: August 20, 2024 Published: October 23, 2024 doi: 10.17675/2305-6894-2024-13-4-10

Keywords: *gravimetric, plant-based inhibitor, concrete corrosion, polarization.*

1. Introduction

Reinforced concrete infrastructures, abbreviated as ReCIs, are widely utilized in modern engineering and construction sectors due to their exceptional ability to withstand heavy loads and harsh environmental conditions. Their durable nature ensures that these structures have a long lifespan, making them a choice for various construction projects [1]. However, ReCIs, despite their strength and durability, are prone to a significant drawback: the rapid corrosion of the reinforcing materials when they come into contact with corrosive atmospheres, such as those containing high amounts of salt or pollutants. This corrosion can

weaken the structure and necessitate costly maintenance and repairs [2]. The corrosive atmospheres in marine environments, with high levels of chloride ions, and polluted atmospheres in industrial and urban areas, with excessive CO_2, sulfate, and sulfide gases [3], cause the pH of concrete aggregates to drop from 12.5–13.5 to less than 10 [4]. When the pH of the concrete mix falls below 10, it leads to corrosion of reinforcing metal (ReM) in the concrete [5]. The passivity of the reinforcing steel is contingent upon the OH concentration of the concrete pore solution. Several sources have indicated that passivity breaks down when the Cl^- to OH^- ratios exceed a specific threshold chloride concentration [6]. Beyond this threshold, the corrosion process is accelerated [7]. These are the main reasons for the rapid degradation of reinforced concrete structures through rust formation on the surface of ReM instead of the formation of protective diffusion barrier passive films [8].

Therefore, one of the inherent limitations of structural infrastructures constructed from reinforced concrete is the gradual deterioration of the metallic reinforcement in urban cities of Nepal [9, 10]. Over time, ReM interactions with the surrounding environment result in corrosion damage, which weakens the reinforcement and ultimately threatens the structural integrity of the ReCIs [11]. Failure to address this issue can lead to costly repairs, pose safety risks, and shorten the lifespan of the structural infrastructures [12]. Therefore, it is essential to implement appropriate measures to prevent, mitigate, or repair corrosion of ReCIs [13]. Various strategies have been employed, including electrochemical removal of chlorine [14], re-alkalization of concrete [15], cathodic protection methods [16, 17], and the use of inhibitors.

Among these corrosion-preventative methods for the ReCIs, corrosion-inhibiting substances like inorganic compounds [18, 19], synthetic organic compounds [20, 21], or phyto-molecules [22] act as concrete additives to mitigate reinforcement concrete corrosion. Corrosion-inhibiting substances are distinguished by their high effectiveness, eco-friendliness, and cost-efficiency [23, 24]. Comparatively, synthetic organic compounds have gained favor as corrosion inhibitors over most inorganic compounds due to their toxic nature and reduced environmentally benign characteristics [25]. However, more efficient, non-toxic, and environmentally friendly phyto-molecules can be extracted from different plant parts (*e.g.*, leaves, barks, stems, roots) and utilized to create plant extracts for corrosion inhibition of metals in corrosive electrolytes [26, 27]. Phyto-molecules having aromatic rings, unsaturated π-systems, and heteroatoms in plant-based extract play a pivotal part in preventing the deterioration of steel rebar embedded in a concrete composite [28, 29].

In recent years, several research groups such as Bhattarai *et al.* [13], Somai *et al.* [22], Ahmed and Ganesh [30], Ghoreishiamiri *et al.* [31], and Valdez-Salas *et al.* [32] have focused on using plant-based phytochemicals as green additives in reinforcement concrete to control their early corrosion damage. These green concrete additives proved to be effective in controlling reinforcement concrete corrosion to a reasonable extent [30]. Conducting anti-corrosion tests on the reinforcement steel rod in concrete composites or in simulated concrete pore solution with plant-based extracts provides some insight into the binding strength of the green inhibitors. More research reports presumed that the plant-based green corrosion

inhibitor shows better adhesion to corroding metal ions in aqueous electrolytes, including in concrete and simulated concrete pore solutions [33]. Besides, a significant research focus on the use of leaf extracts from *Fatsia japonica* [34], *Urtica dioica* [35], and *Platanus acerifolia* [36] plants to inhibit the corrosion of steel in chloride-contaminated concrete. Therefore, the current study aimed to assess the effectiveness of leaf extracts from the endemic species *Ziziphus budhensis* (LEZB) and *Tagetes erecta* (LETE) as environmentally friendly corrosion inhibitors in simulated concrete pore solution (SCP).

In a prior investigation, the *Tagetes erecta* plant was employed in phytoremediation technology to eliminate toxic Zn, Cd metals [37], and styrene [38] from contaminated soils. The flower extract of the plant has demonstrated efficacy as a corrosion inhibitor in marine environments [39] and under acidic conditions [40, 41]. On the contrary, its leaf extract, extracted from leaves, is not utilized as a corrosion inhibitor in concrete. On the other side, different concentrations of *Ziziphus mauritiana* fruit extract in HCl solution showed high anti-corrosive properties to control the corrosion of Al and Cu metals at room temperature from the weight loss method. The inhibition efficiency was increased with the concentration of the inhibitor, reaching a maximum of 76.8% for Al and 88.58% for Cu at a concentration of 1.288 g/L *Z. mauritiana* fruit extract following the Langmuir's adsorption isotherm for both metals [42]. However, among the seven species reported in Nepal, the *Ziziphus budhensis*, a newly identified species within the Rhamnaceae family, has been exclusively documented in Nepal [43]. To the best of the author's knowledge, the potential anti-corrosive properties of *Ziziphus budhensis* and *Tagetes erecta* leaf extracts in reinforced concrete structures have been obscure previously, signifying the novelty of this study.

In this context, the present study intends to investigate the efficacy of leaf extracts derived from *Ziziphus budhensis* (LEZB) and *Tagetes erecta* (LETE) plants as environmentally benign corrosion inhibitors in a saturated $Ca(OH)_2$ solution, presumed as simulated concrete pore (SCP) solution having pH around 11.5. The primary objective is to assess the feasibility of LEZB and LETE as eco-friendly corrosion inhibitors in SCP solutions. In this regard, the study aims to evaluate the effectiveness of both the plant-based inhibitors in protecting MiSR in the SCP solution through gravimetric and electrochemical tests. The findings can offer valuable insights for implementing such inhibitors in concrete.

2. Materials and Methods

The leaves of the *Ziziphus budhensis* [Figure 1a], and *Tagetes erecta* plants [Figure 1b] were collected and authenticated at the National Herbarium and Plant Laboratory of the Plant Department in Godavari, Lalitpur. Subsequently, the leaves were separately dried, pulverized to make powder form, and soaked in methanol at a 1:2 ratio for two weeks with regular stirring, as illustrated in Figure 1c. Then, the supernatant was filtered and evaporated using a rotary evaporator [Figure 1d], as described elsewhere [44], to obtain a semi-solid form of both plant extracts separately. The semi-solid extracts of *Ziziphus budhensis* and *Tagetes erecta*, abbreviated as LEZB and LETE, respectively, were stored at 4°C.

The LEZB or LETE was added into a saturated $Ca(OH)_2$ solution to prepare a distinct series of SCP solutions, each with a pH level of approximately 11.5. There are no significant changes in the initial pH of the SCP solution with the addition of the required amounts of each plant extract. However, the pH values of the test solutions decrease slightly between 10.5 and 11.0. Hence, the SCP solution changes regularly by replacing the fresh solution during the corrosion test until 2802 h to maintain the approximate 11.5 pH. It is meaningful to mention the gravimetric tests and electrochemical measurements carried out in triplicate.

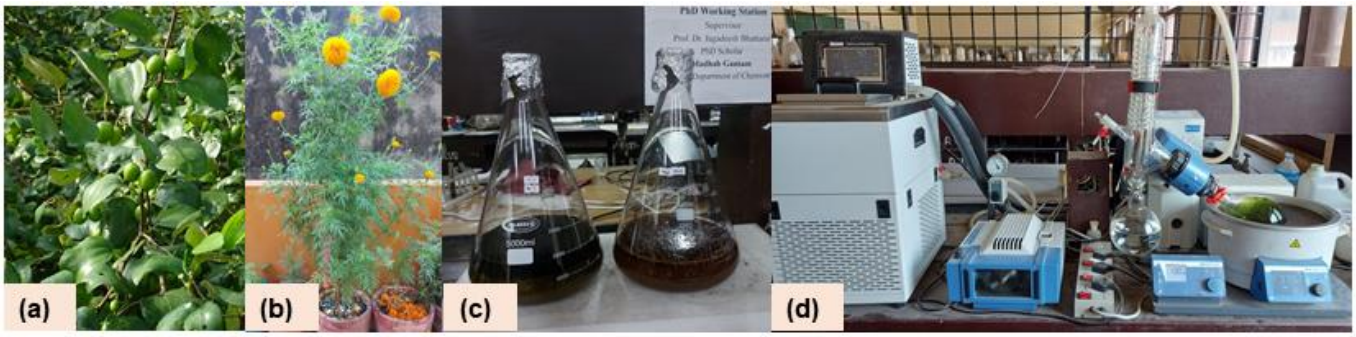

Figure 1. Photographs showing leaves of (a) *Ziziphus budhensis* and (b) *Tagetes erecta* plant, (c) soaking of pulverized leaf powder, and (d) rotary evaporator for removal of solvent.

Twenty-seven rust-free and corrugated 500 XD mild steel rods (MiSRs), each with an average diameter of 113 mm, were prepared for gravimetric analysis, as discussed elsewhere [45]. The weight % composition of the elements constituted in the MiSR is 0.17–0.23% C, 0.70–0.90% Mn, and 0.035% P with about 98% Fe [46]. The initial weights of these specimens were recorded meticulously using a 5-digit micro-balance with an accuracy of 0.00001 grams. Among 27 MiRS samples, three were submerged individually in three 100 mL beakers, each containing 50 mL of SCP solution without LEZB or LETE, which served as the control SCP solution. The remaining 24 samples were dipped individually in three 100 mL beakers, each containing 50 mL of SCP solution with 500, 1000, 2000, and 4000 ppm LEZB and LETE for about four months (*i.e.*, 2802 h). The steel rod pieces were subjected to regular weight measurements using a digital micro-balance at 7, 14, 28, 43, 60, 90 and 118 days while exposed to each SCP solution. Before estimating the weight loss of the corroded sample specimens, the corroded surface is gently brushed with a fine brush and washed with distilled water to remove the corrosion products. This process helps to calculate the corrosion rate more accurately. This procedure is carried out for all sample specimens. Subsequently, the corrosion rate (*CoR*) of MiSR specimens in control SCP solution ($CoR_{control}$) or in SCP solution with LEZB or LETE ($CoR_{inhibit}$) and the corrosion inhibition efficiency (*CoIE*) calculated [47], using the formula given in Equations 1 and 3, respectively.

$$CoR_{\text{Control/Inhibitor}}(\text{mm/y}) = \frac{\Delta w(\text{g}) \cdot 87600}{A(\text{cm}^2) \cdot \rho(\text{g/cm}^2) \cdot t(\text{hr})} \quad (1)$$

$$\theta = \frac{CoR_{\text{control}} - CoR_{\text{inhibitor}}}{CoR_{\text{control}}} \tag{2}$$

$$CoIE(\%) = \frac{CoR_{\text{control}} - CoR_{\text{inhibitor}}}{CoR_{\text{control}}} \cdot 100 \tag{3}$$

where Δw = weight lost after immersion for t hours, A = area of the MiSR specimen calculated using the $2\pi r \cdot (r+l)$ formula, ρ = density of MiSR (7.86 g/cm³), and θ = surface coverage. The surface coverage (θ) calculation depends on the assumption that the LEZB and LETE extracts, used as corrosion inhibitors, prevent iron dissolution entirely in the SCP solution [48].

Similarly, the electrochemical analysis was accomplished through a potentiodynamic polarization (PDP) study, as explained elsewhere [49]. The PDP studies were performed in the potential range of −750 to 1 mV with a scan rate of 20 mV/min. The PDP measurements were conducted three times using three sample specimens for each set of test solutions after immersion of the specimen for 1 hour to record the corrosion potential. The resultant PDP curves exhibited consistent characteristics with nearly identical corrosion potentials. In the aftermath of PDP, the corrosion current density, i_{corr} (A/cm^2), corrosion potential, *CoP* (mV *vs*. SCE), anodic slope, β_a (mV/dec), and cathodic slope, β_c (mV/dec) determined from the anodic and cathodic Tafel plots, as briefed elsewhere [50]. The linear Tafel plots extrapolated within the ±50 mV to calculate the *CoR* based on the i_{corr} (CoR_{icorr}) and the *CoIE* based on the i_{corr} ($CoIE_{\text{icorr}}$), following Equations 4 and 5, respectively [51, 52]. Furthermore, thermodynamic parameters, determined from the linear fit plots of the Langmuir adsorption model [53], are presented in Equation 7.

The linear Tafel plots extrapolated within the 50 mV range from the *CoP*:

$$CoR_{\text{icorr}} = 0.13 \cdot i_{\text{corr}} \cdot \frac{E}{\rho} \tag{4}$$

$$\theta_{\text{icorr}} = \frac{i_{\text{corr(control)}} - i_{\text{corr(inhibitor)}}}{i_{\text{corr(control)}}} \tag{5}$$

$$CoIE_{\text{icorr}}(\%) = \frac{i_{\text{corr(control)}} - i_{\text{corr(inhibitor)}}}{i_{\text{corr(control)}}} \cdot 100 \tag{6}$$

$$\frac{C_{\text{LEZB/LETE}}}{\theta} \text{ or } \frac{C_{\text{LEZB/LETE}}}{\theta_{\text{icorr}}} = \frac{1}{K_{\text{ads}}} + C_{\text{LEZB/LETE}} \tag{7}$$

where E = equivalent weight (55.85), $C_{\text{LEZB/LETE}}$ = concentration of LEZB or LETE extract, θ_{icorr} = surface coverage calculated based on the i_{corr}, K_{ads} = adsorption equilibrium constant. The free energy change ($\Delta G^{\circ}_{\text{ads}}$) can be calculated from K_{ads} using the formula $\Delta G^{\circ}_{\text{ads}} = -2.303RT \cdot \log(55.55 \cdot K_{\text{ads}})$.

Besides the Langmuir adsorption model (LAM), the inhibiting action of phyto-molecules of both plant extracts is elucidated using the Temkin adsorption model (TAM) [54], as depicted in Equation 8. Within Equation 8, the Temkin equilibrium constant (KE_{Tem}) and constant B_{Tem} ($RT/\Delta H_{\text{ads}}$) offer insights into the binding energy and change of heat (ΔH_{ads}) [33], respectively, as in Equation 9. Also, a linear relationship, consistent with the TAM, is observed when plotting θ against log[C_{LEZB}] or log[C_{LETE}] [55].

$$\theta = B_{\text{Tem}} \log\left[KE_{\text{Tem}} \right] + B_{\text{Tem}} \log\left[C_{\text{LEZB}} \text{ or } C_{\text{LETE}} \right] \tag{8}$$

$$\theta = \frac{RT}{\Delta H^{0}_{\text{ads}}} \left(\log KE_{\text{Tem}} + \log C_{\text{LEZB/LETE}} \right) \tag{9}$$

The functional groups of LEZB and LETE were confirmed from FT-IR spectra (IR Affinity-1S, Shimadzu Corp., Japan). Phytochemical tests on LEZB and LETE were conducted to confirm which secondary metabolites were present (+) or absent (−). Besides, the morphological and compositional changes on the MiSR surface, after immersion for 2802 h in SCP without and with 2000 ppm of LEZB or LETE, were analyzed using a scanning electron microscope (Thermo Fisher Scios Field Emission-USA, 10 KV) in connection with an energy dispersive X-ray spectroscope (EDAX Octane Elect EDS/EDX detector-USA, 30 KV). Also, the MiSR sample specimens were analyzed to capture 3D surface images and roughness using a white light interferometer (NewView-9000, Zygo Corporation).

3. Results and Discussion

Primary screening tests confirmed the presence (+) or absence (−) of different secondary metabolites on LEZB and LETE extracts from corresponding testing methods, as described elsewhere [55]. The secondary metabolites of LEZB and LETE are heteroatoms, unsaturated π-electrons, or aromatic rings containing secondary phyto-molecules (alkaloids, flavonoids, glycosides, phenols, tannins, and terpenoids). The results obtained from the chemical screening tests for LEZB [56, 57] and LETE [58, 59] are consistent with the findings documented in the existing literature. These phyto-molecules of LETE and leaf extract of *Ziziphus* species can form a diffusion barrier passive layer on the reinforcing steel (rebar) surface through adsorption. It protects the rebar corrosion and is consistent with previous literature [60].

The FTIR spectra shown in Figure 2a and 2b indicate the identification of functional groups in LEZB and LETE, respectively. These are characterized by the FTIR peak values, at approximately 3363–3340 cm^{-1} for O–H stretching vibration in aromatic compounds [40], 1730–1715 for C–H or C=O stretching vibration [61], 1605 cm^{-1} for aromatic C=C stretching [62], 1457–1450 cm^{-1} for C–H stretching [63], 1256 cm^{-1} for C–O stretching and C–H stretching at 1038–1026 cm^{-1} for O–H or C–H bending of aromatics [64].

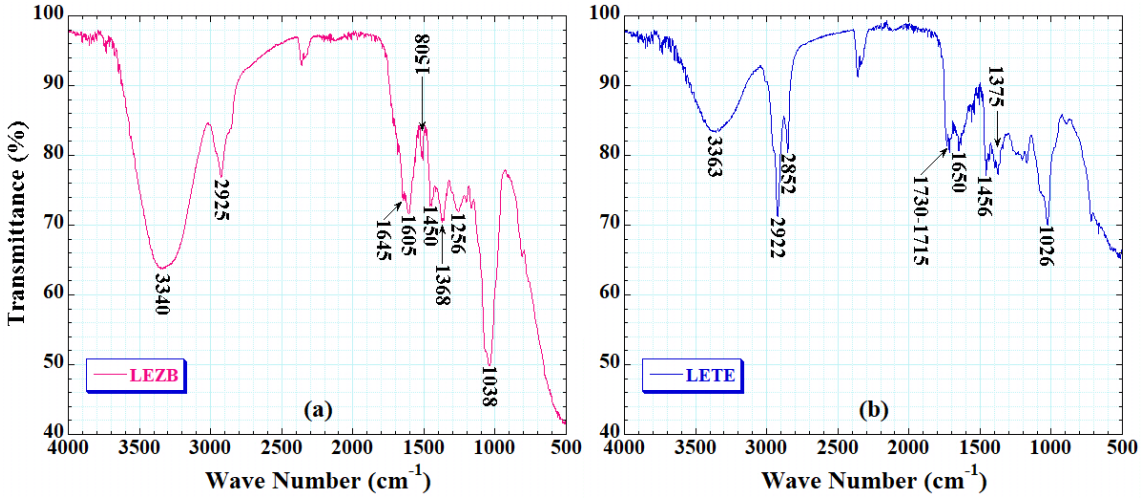

Figure 2. FTIR spectra of (a) LEZB and (b) LETE.

Based on the estimated corrosion rate of MiSR, the inhibition efficiency was studied using two methods. The first method is gravimetric (weight loss), and the second is electrochemical polarization. The gravimetric method is convenient for examining adsorption mechanisms, whereas the potentiodynamic polarization provides the corrosion inhibition kinetics of MiSR specimens in the SCP solution. The corrosion rates from the gravimetric analysis shown for the MiSR immersed in SCPs without (*i.e.*, control specimen) and with 500–4000 ppm LEZB and LETE, as illustrated in Figures 3a and 3b, respectively, as a function of immersion time. These figures demonstrate that the corrosion rate of MiSR decreases with the addition of LEZB or LETE concentrations from 500 to 4000 ppm in SCP solution, compared to SCP without inhibitors. Explicitly, the corrosion inhibition effect of the LEZB in the SCP solution is remarkably higher than the LETE, indicating more effective corrosion prevention for the MiSR, with increasing concentrations of LEZB in the SCP, as illustrated in Figure 3a.

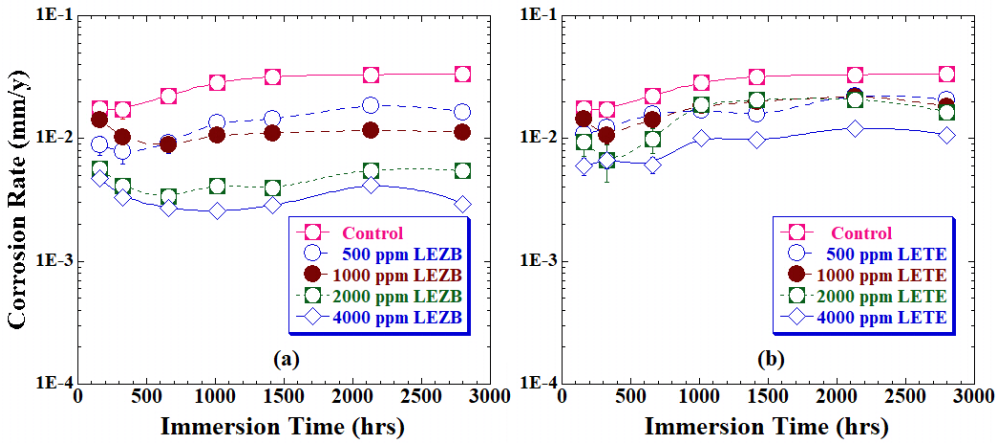

Figure 3. Variation of corrosion rate of MiSR in SCP solution without and with different concentrations of (a) LEZB and (b) LETE.

Furthermore, Figures 4b and 4b show the changes in the corrosion inhibition efficiencies (*CoIE*) of both LEZB and LETE extracts on the MiSR in SCP solution. In the addition of 500–1000 ppm of both the plant extracts in SCP, the *CoIE* increased at a steep angle, and it increases moderately with further increase in the extract concentrations, showing maximum *CoIE* at 4000 ppm LEZB or LETE in SCP solution for MiSR. The highest corrosion inhibition efficiency (*CoIE*), reaching 91.22%, was observed after immersing the MiSR for 2802 hours in a solution containing 4000 ppm of LEZB.

A similar trend was observed in the corrosion resistance performance of SCP solution with 4000 ppm of LETE, reaching a maximum of 67.81% *CoIE*. A previous study reported that the adsorption of $Ca(OH)_2$ increases donor density and vacancy flux, reduces the defects diffusion coefficient, and accelerates the oxidation of Fe(II) to Fe(III) [65]. It aids in forming a new passive film with improved resistance to corrosion. We anticipate that the presence of plant-based extracts significantly influences the nucleation and growth of the passive film formation when $Ca(OH)_2$ is involved.

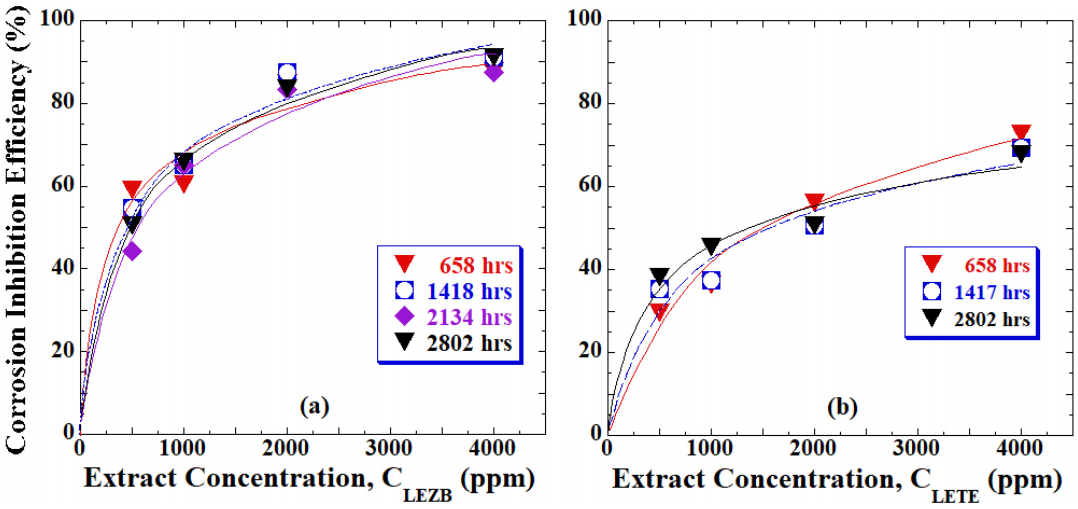

Figure 4. Variation of corrosion inhibition efficiency of MiSR in SCP solution with 500–4000 ppm of (a) LEZB and (b) LETE at different immersion times.

The leaf-derived extracts of LEZB and LETE, as reported from the chemical screening tests, consist of a diverse array of secondary phyto-molecules, including alkaloids, flavonoids, glycosides, phenols, and terpenoids. These secondary phyto-molecules, comprised of heteroatoms and π-electrons ring compounds, are postulated to act as focal points for interaction with the corroded surfaces of MiSR in a SCP solution with a strongly alkaline $Ca(OH)_2$ electrolyte [27]. Another study indicated an 89% inhibition efficiency when a 3.5% NaCl-saturated $Ca(OH)_2$ solution was blended with a 4% organic inhibitor [23]. The study confirmed the protective effects for steel by detecting an organic film comprising aromatic groups of the blended-organic inhibitor on the surface of the carbon steel.

Therefore, the corrosion-controlling process of the mild steel in SCP solution with plant-based inhibitors involved the development of a protective passive film on the steel surface [66]. This corrosion-protecting passive film formation is also due to the adsorptive

interaction of phyto-molecules of the plant extract with the steel surface [67]. The LEZB and LETE extracts inhibit corrosion by adsorbing on the corroded MiSR surface, following LAM and TAM. It is essential to recognize that the mechanism is intricate, considering corrosion inhibition by adsorption of phyto-molecules. The multifaceted chemical interactions, encompassing electronic, structural, and steric effects, can potentially arise between the phyto-molecules of the extract and the corroded surface [68].

The LAM and TAM are fundamental adsorption models that elucidate the molecular interaction between inhibitor phyto-molecules and corroded MiSR surfaces. These models operate on the premise of uniformity across adsorption sites and assert that particle binding is independent of the occupancy status of neighboring sites [69]. In particular, the LAM describes the corrosion inhibition mechanism due to its ease of application and provision of sufficient information [70]. It represents a fundamental model for elucidating the interaction between inhibitor secondary phyto-molecules of the plant extracts (*e.g.*, LEZB or LETE) and the corroded-MiSR surface (*i.e.*, Fe^{2+} ions).

The LAM postulates that adsorption sites exhibit uniformity, with particle binding occurring independently, as described elsewhere [53, 71]. Figures 5a and 5b portray the correlation between C_{LEZB}/θ and C_{LEZB} or C_{LETE}/θ and C_{LETE}, respectively, for MiSR after different immersion hours in SCP solution under varying concentrations of LEZB and LETE. The findings reveal a consistent linear coefficient of determination (R^2) close to unity (*i.e.*, between 0.96 and 1.00) across all scenarios. The study evaluated the inhibitory mechanism of *Ziziphus budhensis* or *Tagetes erecta* onto MiSR in SCP solution at 25°C.

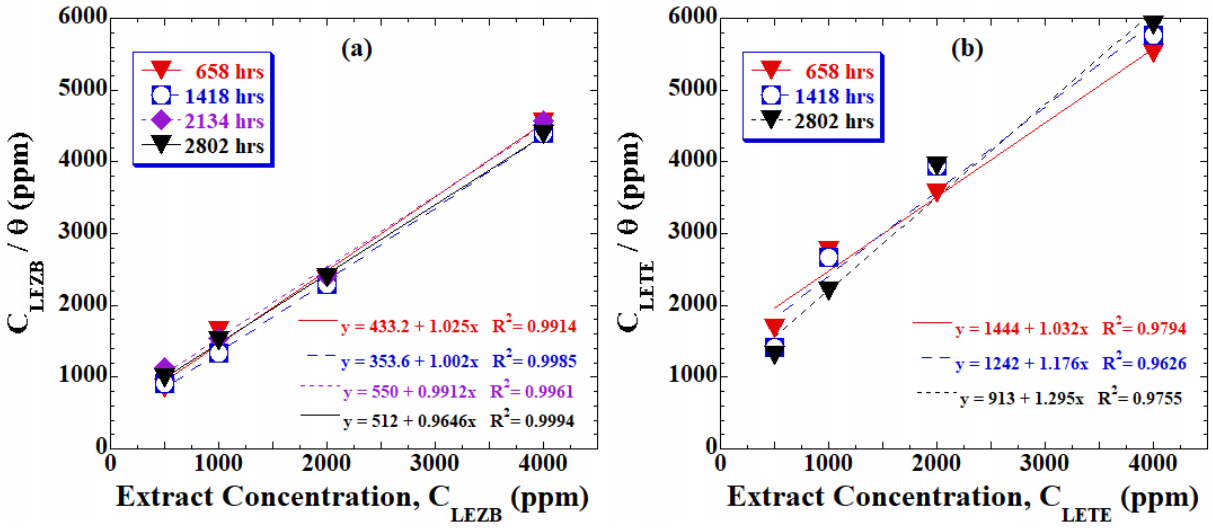

Figure 5. Langmuir plots of MiSR in SCP solution with different concentrations of (a) LEZB and (b) LETE.

To be specific, the TAM believes three assumptions: they are (i) linearly decreases the ΔH_{ads} with coverage rather than logarithmically, (ii) uniformly distributed surface binding energies enhance the adsorption process, and (iii) it accounts for the interaction between the adsorbate and the adsorbent [72, 73]. Upon analysis of data for testing the Temkin isotherm

model, the plots of θ versus log(C_{LEZB}) or θ versus log(C_{LETE}) yielded linear relationships, with corresponding R^2 values falling within the range of 0.86 to 0.98 (*i.e.*, lower than in Langmuir plots), as depicted in Figures 6a and 6b, respectively. These findings substantiate the validity of the Temkin adsorption isotherm in characterizing the adsorption mechanism of LEZB or LETE on MiSR surfaces, thereby exerting control over their corrosion in SCP solution at a temperature of 25±1°C. Additionally, the conformity to the Temkin adsorption isotherm suggests that the adsorption of the plant-based LEZB or LETE corrosion inhibitors likely occurs in a monolayer fashion on the uniformly corroded MiSR surface [74].

However, based on the estimated R^2 values for the Langmuir and Temkin isotherms, it inferred that the adsorption behavior of LEZB and LETE on the corroded MiSR surface conforms most closely to the Langmuir isotherm. Besides, the molecular interaction parameter, influenced by the Temkin equilibrium constant, binding energy, and heat of adsorption as determined from the Temkin isotherm linear fit, has yielded a negative value, which signifies that the adsorbed phyto-molecules from both the LEZB and LETE extracts manifest a repulsive force toward the adsorbing species [75]. The observation aligns with the LAM. Repulsion between adsorbed molecules and adsorbing species primarily fosters monolayer formation of the extract on the MiSR surface.

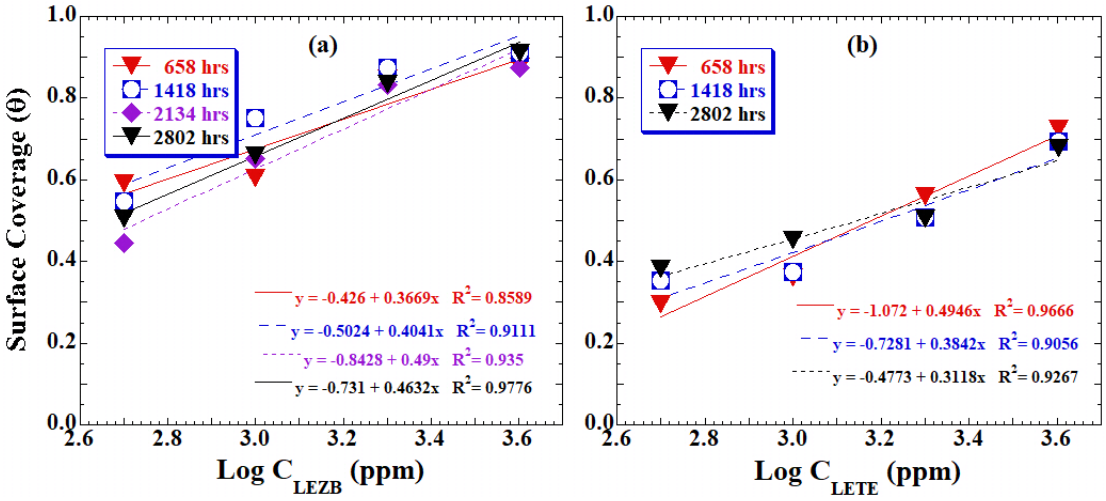

Figure 6. Temkin plots of MiSR in SCP solution with different concentrations of (a) LEZB and (b) LETE.

Demonstrating the LAM as the best fit compared with the TAM, it suggests that the LEZB and LETE-based phyto-molecules adsorbed onto the corroded MiSR surface to form a uniform single-layered protective layer [76]. According to the LAM, there is minimal interaction (*i.e.*, physical adsorption) between the inhibitor molecules and the metal surface [77]. The substantial adsorption of the LEZB and LETE-based inhibitors on the corroded MiSR surface is attributed to the presence of electron-donating atoms such as nitrogen (N), sulfur (S), and oxygen (O) within the phyto-molecular structures of the LEZB and LETE, as confirms from the screening test results above. These atoms of the phyto-molecules can form coordinate bonds with the corroded iron atom [78], thereby facilitating the formation of a

protective passive layer because these phyto-molecules of LEZB and LETE have high shielding effect and corrosion-inhibiting potential against material attack. The observation aligns with the findings of many researchers in their previous findings who documented similar adsorption behavior of plant extracts on metal corrosion in acidic environments [79, 80].

Besides, as described above in Equation 6, the corrosion inhibition efficiency (*CoIE*) of the LEZB and LETE can be approximated using the potentiodynamic polarization (PDP) measurements for studying the adsorption kinetics of LEZB or LETE-based phyto-molecules on MiSR surface in the SCP solution. Figures 7a and 7b depict the PDP outcomes in the form of Tafel plots for MiSR in SCP solution without (control) and with different concentrations of LEZB and LETE inhibitors, respectively. The *CoP* values shifted in the negative direction between the inhibited and control conditions, indicating a blockage of the active cathode sites on the MiSR by the phyto-molecules. Previous works have reported that plant-based phytochemicals can classified as cathodic, anodic, or mixed-type corrosion inhibitors based merely on whether the *CoP* difference between the control and inhibited conditions is more than 85 mV or is not [81]. The observed *CoP* differences exceeding 85 mV (SCE) in this study indicate that the LEZB or LETE inhibitor is cathodic-type, as reported by Sayed *et al.* in 2019 [82].

Following the Tafel extrapolation plots using the linear potential resistant (LPR) method, electrochemical kinetic factors - *CoP*, i_{corr}, β_a, and β_c were determined from the PDP curves and summarized in Table 1. The i_{corr} values in the test SCP solutions containing inhibitors consistently exhibit lower values compared to the control sample. It suggests the development of a protective layer on the MiSR surface, which effectively mitigates the dissolution of Fe^{3+} ions in the SCP solution.

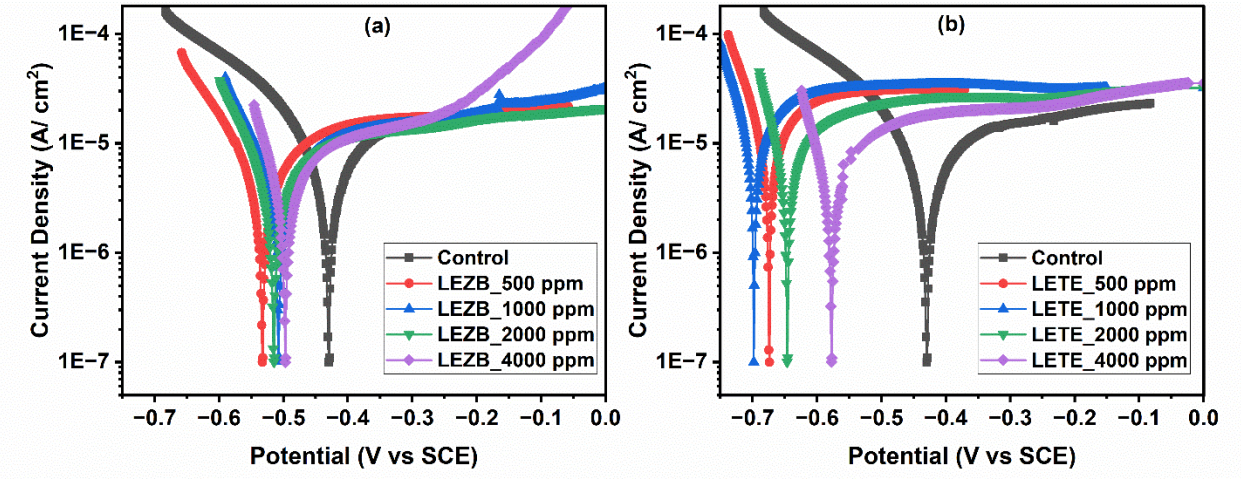

Figure 7. Potentiodynamic polarization curves for MiSR immersed in SCP without and with different concentrations of (a) LEZB and (b) LETE.

Table 1. Gravimetric and electrochemical parameters obtained from weight loss and LPR methods.

	Inhibitor, ppm	**ϕ_{corr}, mV**	***i*$_{corr}$, μA/cm^2**	**β_a, mV/dec**	**$-\beta_c$, mV/dec**	***i*$_{corr}$-based *CoR*, mm/y**	***i*$_{corr}$-based *CoIE*, %**	***Wt.*-based *CoR*, mm/y**	***Wt.*-based *CoIE*, %**
Control	–	–428.4	7.301	2.54	6.33	6.75	–	0.03324	–
LEZB	500	–529.5	3.111	10.33	19.86	2.87	56.74	0.01642	50.61
	1000	–508.4	3.027	12.73	23.13	2.79	58.67	0.01131	65.98
	2000	–514.3	1.925	11.46	25.66	1.78	73.63	0.00546	83.57
	4000	–495.8	1.357	14.88	21.82	1.25	81.48	0.00292	91.22
LETE	500	–673.6	3.606	08.86	15.15	3.33	50.67	0.02052	38.27
	1000	–698.7	3.105	07.46	18.11	2.87	57.48	0.01816	45.37
	2000	–646.9	3.039	12.09	14.61	2.81	58.37	0.01641	50.63
	4000	–576.2	1.918	06.21	27.33	1.77	73.78	0.01070	67.81

Furthermore, akin to the *CoP* values, the cathodic slope values did not exhibit a distinct regular trend of change with extract concentrations, suggesting that both extracts could impede corrosion through the adsorption process on the MiSR surface. The shift in *CoP* values of the MiSR in the SCP solution with plant extract concentrations, compared to the control SCP solution, indicates a blockage of active sites on the MiSR by phyto-molecules of LEZB and LETE extracts.

The introduction of LEZB and LETE to the SCP solution caused a significant shift in the *CoP* values towards more negative values concerning the *CoP* of the MiSR in the control SCP solution, as illustrated in Figure 8. There is no discernible trend in the *CoP* and cathodic current density (i_c) as the extract concentration increased, providing further evidence that both plant extracts functioned as mixed-type corrosion inhibitors even though the *CoP*s of the MiSR in all concentrations of LEZB or LETE located between the *CoP* in control and 500 ppm LEZB or LETE extract. The findings demonstrate that the plant base LEZB and LETE inhibitors effectively mitigate the corrosion rate, operating as a cathodic-type inhibitor with predominant control over the cathodic reaction, as described in previous works [83]. The additions of either LEZB or LETE extract in the SCP solution enhance a decrease in the i_{corr} value, suggesting the formation of a passive layer on the surface of the MiSR. The plant extracts addition enhances the potential for protecting corroded MiSR in SPC solution, as evidenced by the decreased corrosion rate (*CoR*) and increased inhibition efficiency (*CoIE*%) values. The highest inhibition efficiency (*i.e.*, 81.48%) in SCP solution with 4000 ppm LEZB compared with other concentrations of both extracts. These findings from electrochemical tests align closely with those obtained from gravimetric tests, indicating that the 4000 ppm of LEZB extract could be an effective corrosion inhibitor for concrete additives.

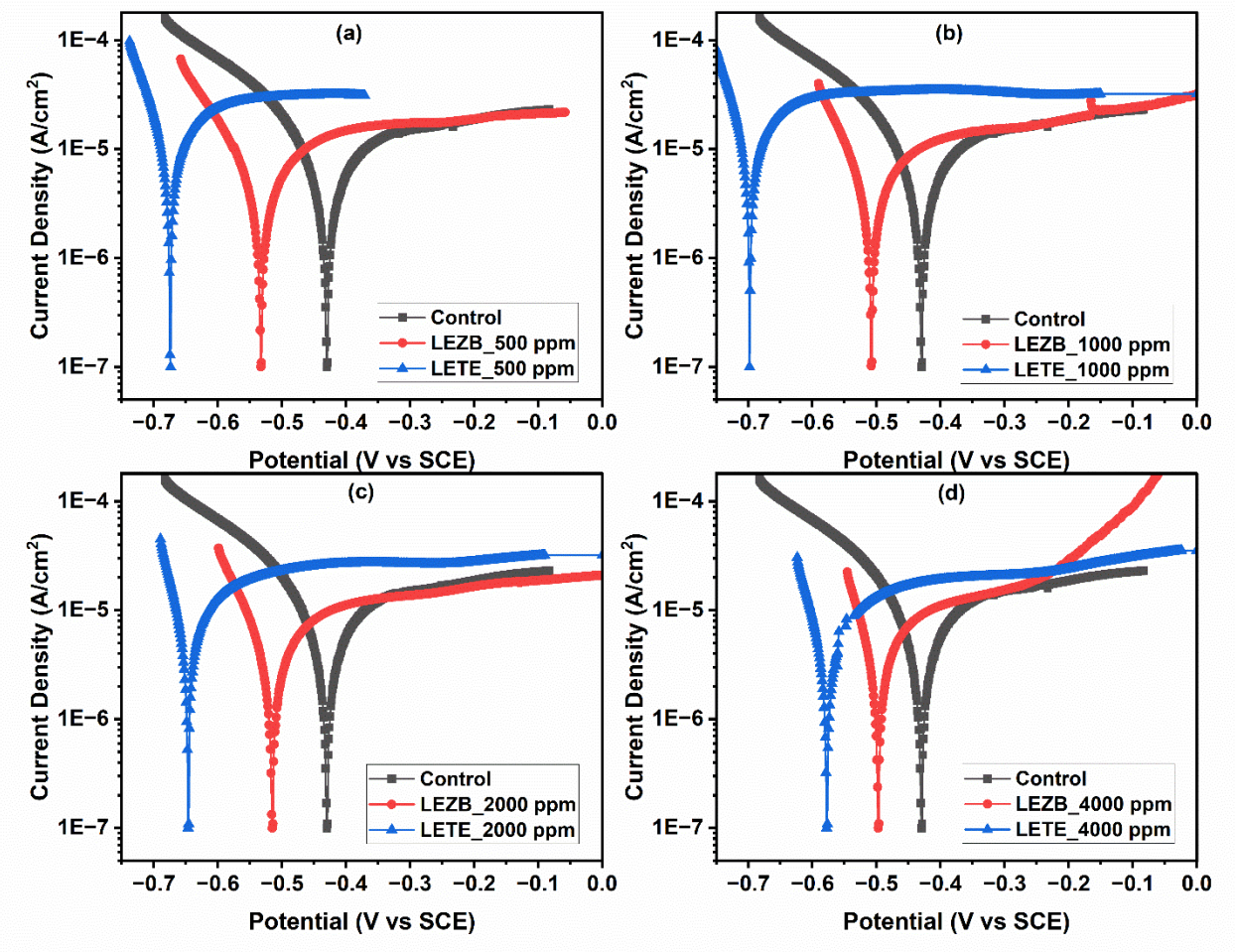

Figure 8. Potentiodynamic polarization curves for MiSR immersed in SCP with (a) 500 ppm, (b) 1000 ppm, (c) 2000 ppm and (d) 4000 ppm LEZB and LETE including blank (control).

SEM technique was employed to analyze the changes in the surface morphology of MiSR before and after immersion for 2802 h in SCP solutions without (control) and without 2000 ppm LEZB or LETE extract inhibitor. In the control SCP solution without the extract inhibitors, the MiSR surface severely corroded and the surface covered by thick corrosion products, hence causing significant damages, as illustrated in the SEM image in Figure 9. The corroded layer looked rough and porous with cracks, allowing aggressive ions to penetrate deeply into the MiSR surface, and hence showed a significantly high corrosion rate of the MiSR after immersion for 2802 h in control SCP solution, as noticed in Figures 3a and 3b.

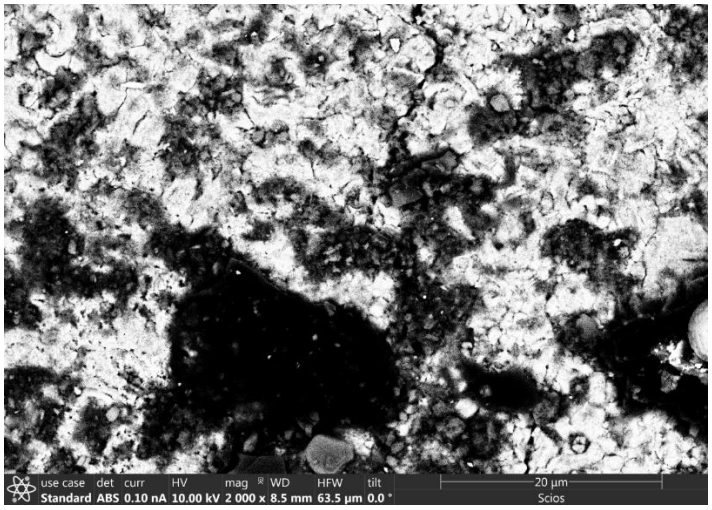

Figure 9. SEM image of the surface layer formed on MiSR after dipping it for 2802 h in the control SCP solution without extract.

In contrast, after 2802 h of immersion in SCP with 4000 ppm LEZB and LETE, the MiSR surface showed minimal damage and a relatively even surface, as demonstrated in Figure 10a and 10b, respectively. Both SEM images confirm that very few corrosion products formed with smooth morphologies, suggesting the anti-corrosion activities of LEZB and LETE in the SCP solution. The protective layer formed on the surface of MiSR in the SCP solution with LEZB and LETE extracts acts as a shielding agent to protect the MiSR from aggressive environments, as described elsewhere [84]. Moreover, SEM images illustrate a micro-image of the MiSR surface obtained from the control SCP solution, revealing multiple oxide films that point to a high rate of iron oxidation in the SCP solution. This finding aligns with the low weight percentage (*wt*.%) of iron and high oxygen content identified through energy dispersive X-ray spectroscopy (EDS) analysis. Conversely, the MiSR retrieved from the inhibited SCP solution containing 4000 ppm LEZB and 4000 ppm LETE exhibits smooth surfaces devoid of pits and cracks, as depicted in Figures 10a and 10b, respectively.

Based on the EDS analysis results, the exposed MiSR sample for 2802 h in the control SCP solution exhibited an elemental Fe content of 55.47% with a high oxygen concentration of 31.53%, which indicates a notable corrosion reaction on the MiSR surface in the control SCP solution (Figure 9). Conversely, minimal corrosion was observed on the MiSR surface when immersed in the SCP solution containing 4000 ppm LEZB [Figure 10a] and 400 ppm LETE extract [Figure 10b], resulting in 69.76% and 68.10% iron and oxygen concentrations of 23.21% and 24.01%, respectively, as tabulated in Table 2. The results summarized in Table 2 suggest effective inhibition of iron dissolution from the MiSR in SCP solution with varying concentrations of LEZB and LETE additions. Consequently, it said that the low oxygen with high iron content indicates the MiSR surface is less corroded with comparatively low amounts of rust, thereby minimizing iron loss in SCP solution with

4000 ppm LEZB or LETE from the EDS analysis. Similar properties have been documented in prior research [85, 86].

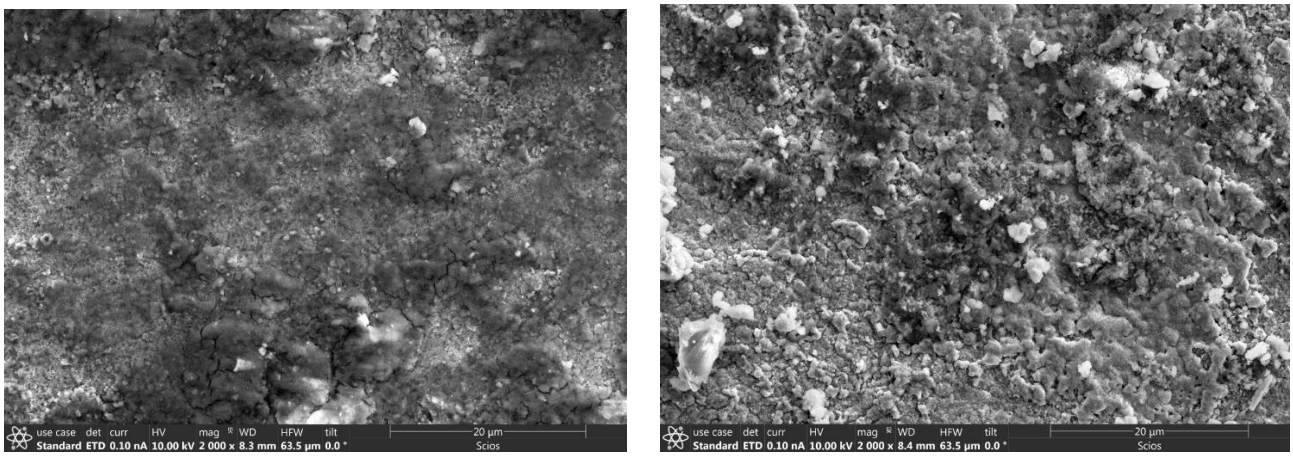

(a) (b)

Figure 10. SEM images of MiSR layer formed after 2802 h immersion in SCP with 4000 ppm of (a) LEZB and (b) LETE.

Table 2. EDS analysis of the MiSR surface after 2802 hours immersion in control SCP solution and SCP with 4000 ppm LEZB and LETE including the composition of a fresh MiSR surface.

Elements	Composition (*wt.*%) of immersed-MiSR for 2802 h in SCP solution			Fresh MiSR (wt.%)
	at control condition	with 4000 ppm of LEZB	with 4000 ppm LETE	
O K	31.53	23.21	24.01	–
Fe K	55.47	69.76	68.10	98.27–98.35
Al K	–	01.52	–	–
Ca K	07.09	03.01	03.45	–
Si K	03.01	02.41	01.50	0.40
Na K	02.90	–	02.94	–
C	–	–	–	0.17–0.25
Misc.	–	–	–	1.08

In addition to conducting SEM/EDS analysis, we employed the three-dimensional (3D) topography technique of white light interferometry (WLI) to examine the 3D white-light interference images of the tested specimens. White light interferometry (WLI) gives fast, accurate, non-contact surface topography in three dimensions (3Ds). It is an advanced, non-destructive optical surface profiling technique that provides exceptional lateral and vertical resolution for precise materials characterization [87]. The white-light interferometers

(WLIs) have garnered considerable attention from researchers over the past few decades due to their exceptional precision, 3D surface mapping capabilities, color display functionality, aptitude for measuring surface roughness, and microscale components, and so on [88]. It could successfully resolve the surface profile of test structures even for a smooth surface with a roughness of a few angstroms [89]. The method is one of the widely used corrosion studies [90, 91], and its sensitivity is sufficient for studying rebar concrete corrosion [92].

These advantages of the WLI are also exploited in the present study to examine the 3D white-light interference images of the tested MiSR specimens. These specimens underwent preparation for WLI analysis after immersion for 2802 h in control SCP solution and SCP solutions with 2000 ppm LEZB and LETE. Figures 11–13 yield valuable insights into these MiSR specimens' 3D topographical surface characteristics. Upon immersion in the control SCP solution, the MiSR exhibited a surface roughness (SR) of 8.501 µm, attributed to significant corrosion (Figure 11). Notably, the SR values for MiSR specimens immersed in SCP solutions containing 2000 ppm LEZB (Figure 12) and LETE (Figure 13) for 2802 h are 3.904 µm and 5.727 µm, respectively. These measurements represent a 54.08% and 32.63% reduction in SR relative to the control SCP solution. The LEZB and LETE demonstrate superior inhibitive characteristics and show consistency with the corrosion morphology analysis from SEM/EDS techniques.

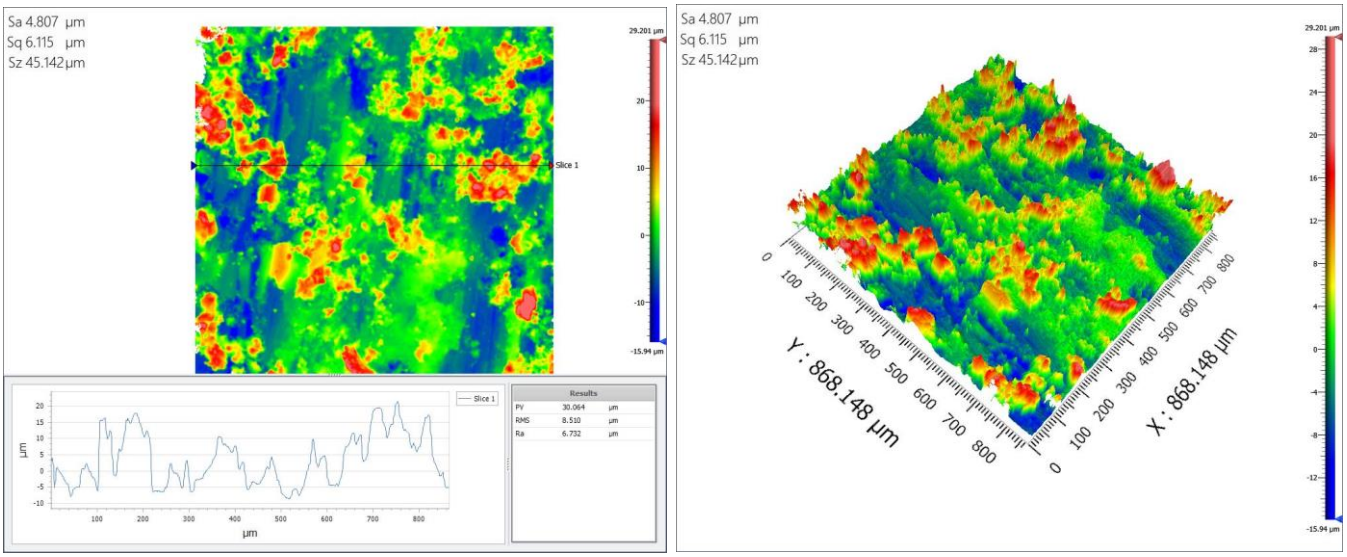

Figure 11. 2D (upper) and 3D (lower) topographical WLI images of MiSR surface formed after immersion for 2802 h in control SCP solution.

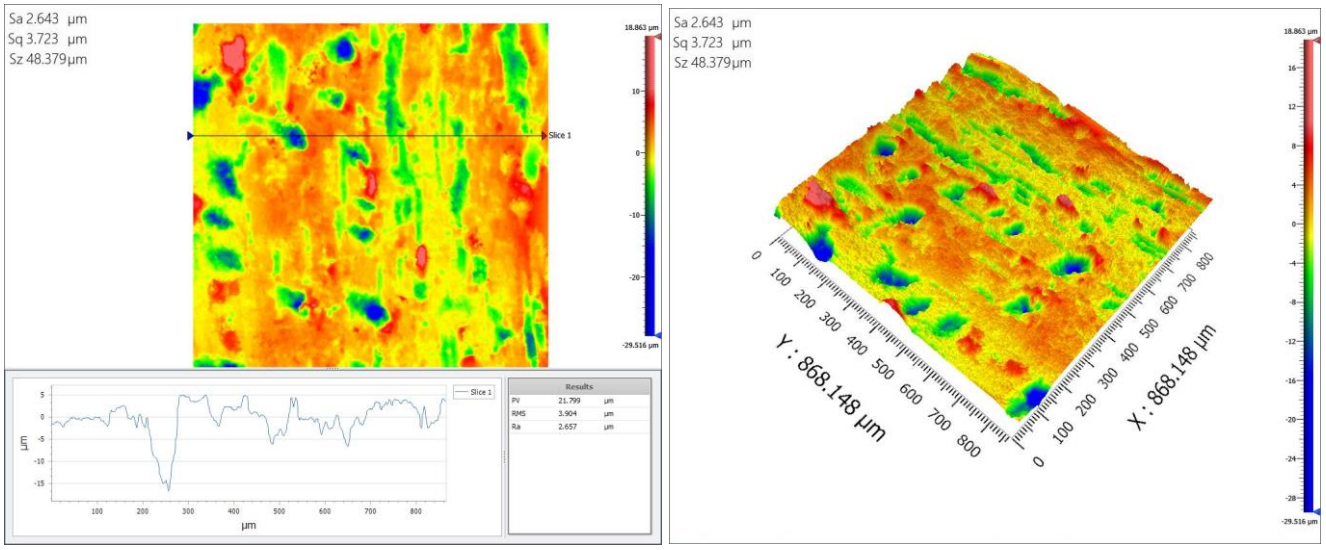

Figure 12. 2D (upper) and 3D (lower) topographical WLI image of MiSR surface formed after immersion for 2802 h in SCP solution with 2000 ppm LEZB.

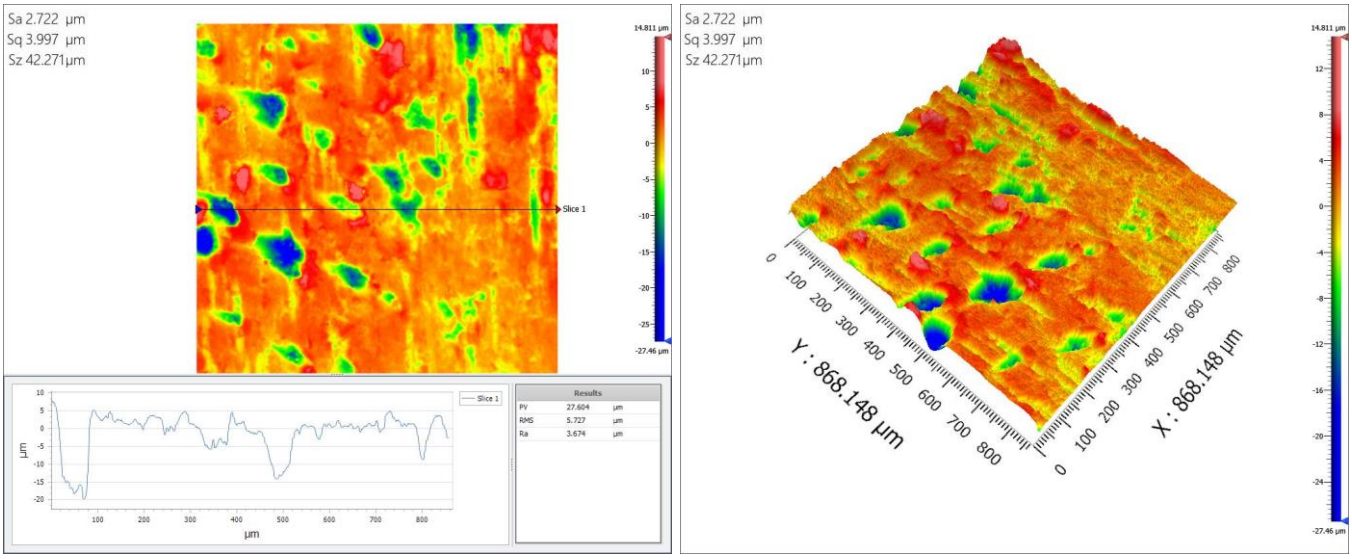

Figure 13. 2D (upper) and 3D (lower) topographical WLI image of MiSR surface formed after immersion for 2802 h in SCP solution with 2000 ppm LETE.

3. Conclusions

Based on the gravimetric weight loss, electrochemical, and surface analysis tests, as the knowledge of the authors, for the first time, this study shows that plant extracts (LEZB and LETE) effectively inhibit corrosion of the mild steel rod (MiSR) exposed to simulated concrete pore (SCP) solution. The extracts create protective surface layers, reducing the corrosion rate of the MiSR. The inhibition efficiencies reached optimal of 91.22% and 81.48% when utilizing 4000 ppm of LEZB and 73.78% and 67.81% with 4000 ppm LETE in the concrete pore solution at ambient temperature. These values were determined using weight loss and potentiodynamic polarization (PDP) analysis techniques. The PDP

measurements confirmed that the LEZB and LETE act as cathodic-type inhibitors with predominant control by the cathodic reaction. The extract-based phyto-molecules adsorbed onto the corroded MiSR surface to form a uniform single-layered protective layer according to the Langmuir and Temkin adsorption isotherm models. Surface analysis using SEM/EDS and WLI showed that the MiSR surface after being immersed in SCP with plant extracts is smooth, compared to the MiSR sample immersed in the control SCP solution without LEZB/LETE. Additionally, EDX analysis confirmed that LEZB and LETE additions in the SCP solution protected the MiSR. This finding motivates researchers to investigate the anti-corrosive characteristics of novel plant-based extracts as additives in concrete.

Acknowledgements

The University Grants Commission (UGC-Nepal) for providing a UGC Ph. D. Research Award No.: PhD-78/79 S&T-03 to MG.

References

1. T.A. Hemkemeier, F.C. Almeida, A. Sales and A.J. Klemm, Corrosion Monitoring by Open Circuit Potential in Steel Reinforcements Embedded in Cementitious Composites with Industrial Wastes, *Case Stud. Constr. Mater*., 2022, **16**, e01042. doi: 10.1016/j.cscm.2022.e01042
2. Z. Song, L. Liu, M.Z. Guo, H. Cai, Q. Liu, S. Donkor and H. Zhao, Inhibition Performance of Extract Reinforcement Corrosion Inhibitor from Waste *Platanus acerifolia* Leaves in Simulated Concrete Pore Solution, *Case Stud. Constr. Mater*., 2024, **20**, e02992. doi: 10.1016/j.cscm.2024.e02992
3. D. Sun, Z. Cao, C. Huang, K. Wu, G. De Schutter and L. Zhang, Degradation of Concrete in Marine Environment Under Coupled Chloride and Sulfate Attack: A Numerical and Experimental Study, *Case Stud. Constr. Mater*., 2022, **17**, e01218. doi: 10.1016/j.cscm.2022.e01218
4. J.P. Broomfield, *Corrosion of Steel in Concrete: Understanding, Investigation, and Repair*, 2nd ed., London, UK, CRC Press, Taylor & Francis Group 2019, 296 pp.
5. M.B. Harb, S. Abubshait, N. Etteyeb, M. Kamoun and A. Dhouib, Olive Leaf Extract as a Green Corrosion Inhibitor of Reinforced Concrete Contaminated with Seawater, *Arabian J. Chem*., 2020, **13**, no. 3, 4846−4856. doi: 10.1016/j.arabjc.2020.01.016
6. M.A. Quraishi, D.K. Nayak, R. Kumar and V. Kumar, Corrosion of Reinforced Steel in Concrete and Its Control: An overview, *J. Steel Struct. Constr*., 2017, **3**, no. 1, 1000124. doi: 10.4172/2472-0437.1000124
7. E. Huttunen-Saarivirta, E. Bohner, A. Trentin and M. Ferreira, A Closer Look at the Corrosion of Steel Liner Embedded in Concrete, *Cem. Concr. Compos*., 2023, **144**, 105280. 10.1016/j.cemconcomp.2023.105280
8. J. Bhattarai, *Frontiers of Corrosion Science* (1st ed.), Kshitiz Publication, Kirtipur, Nepal, 2010, 304 pp.

9. I. Laudari, N.R. Phulara, M. Gautam and J. Bhattarai, Evaluation of Corrosion Condition of Some Steel-Reinforced Concrete Infrastructures Available in Pokhara Valley of Nepal, *Tribhuvan University Journal*, 2021, **36**, no. 1, 1−17. doi: 10.3126/tuj.v36i01.43509
10. N.R. Phulara and J. Bhattarai, Assessment on Corrosion Damage of Steel Reinforced Concrete Structures of Kathmandu Valley Using Corrosion Potential Mapping Method, *J. Inst. Eng*., 2019, **15**, no. 2, 45−54. doi: 10.3126/jie.v15i2.27640
11. J. Wang, Z. Zhang, X. Liu, Y. Shao, X. Liu and H. Wang, Prediction and Interpretation of Concrete Corrosion Induced by Carbon Dioxide Using Machine Learning, *Corros. Sci*., 2024, **233**, 112100. doi: 10.1016/j.corsci.2024.112100
12. C. Andrade, Propagation of Reinforcement Corrosion: Principles, Testing and Modelling, *Mater. Struct*., 2019, **52**, no. 2, 1−26. doi: 10.1617/s11527-018-1301-1
13. J. Bhattarai, M. Somai, N. Acharya, A. Giri, A. Roka and N.P. Phulara, Study on the Effects of Green-Based Plant Extracts and Water-Proofers as Anti-Corrosion Agents for Steel-Reinforced Concrete Slabs, *E3S Web Conf*., 2021, **302**, 02018. doi: 10.1051/e3sconf/202130202018
14. V. Bouteiller, Y. Tissier, E. Marie-Victoire, T. Chaussadent and S. Joiret, The Application of Electrochemical Chloride Extraction to Reinforced Concrete – A Review, *Constr. Build. Mater*., 2022, **351**, 128931. doi: 10.1016/j.conbuildmat.2022.128931
15. A. Karmegam, S. Avudaiappan, M. Amran, P. Guindos, N.I. Vatin and R. Fediuk, Retrofitting RC Beams Using High-early Strength Alkali-activated Concrete, *Case Stud. Constr. Mater*., 2022, **17**, e01194. doi: 10.1016/j.cscm.2022.e01194
16. J. Ha, J. Jeong and C. Jin, Development of Conductive Mortar for Efficient Sacrificial Anode Cathodic Protection of Reinforced Concrete Structures-part 2: Four-year Performance Evaluation in Bridges, *Appl. Sci*., 2023, **14**, no. 5, 1797. doi: 10.3390/app14051797
17. E.K. Arya and B.S. Dhanya, Corrosion Control of Reinforced Concrete Structures in Construction Industry: A Review, *IOP Conf. Ser.: Mater. Sci. Eng*., 2021, **1114**, 012006. doi: 10.1088/1757-899X/1114/1/012006
18. Shehnazdeep, B. Pradhan, A Study on Effectiveness of Inorganic and Organic Corrosion Inhibitors on Rebar Corrosion in Concrete: A Review, *Mater. Today: Proc*., 2021, **65**, 1360−1366. doi: 10.1016/j.matpr.2022.04.296
19. V.S. Reddy, T. Prashanth, V.S.P. Raju and P. Prashanth, Effect of Organic and Inorganic Corrosion Inhibitors on Strength Properties of Concrete, *E3S Web Conf*., 2020, **184**, 01112. doi: 10.1051/e3sconf/202018401112
20. A. Roka, M. Gautam, A. Giri, N.P. Bhattarai and J. Bhattarai, The Anti-degradation Consequences of Water Repellent-based Inhibitors for Controlling Mild Steel Corrosion in Concrete Composite, *E3S Web Conf*., 2023, **455**, 01002. doi: 10.1051/e3sconf/202345501002
21. L. Shen and H. Zhang, Corrosion inhibition and adsorption behavior of (3-aminopropyl)-triethoxysilane on steel surface in the simulated concrete pore solution contaminated with chloride, *J. Mol. Liq*., 2022, **363**, 119896. doi: 10.1016/j.molliq.2022.119896

22. M. Somai, A. Giri, A. Roka and J. Bhattarai, Comparative Studies on the Anti-corrosive Action of Waterproofing Agent and Plant Extract to Steel Rebar, *Macromol. Symp*., 2023, **410**, no. 1, 2100276. doi: 10.1002/masy.202100276
23. P. Wang, Y. Wang, T. Zhao, C. Xiong, P. Xu, J. Zhou and Z. Fan, Effectiveness Protection Performance of an Internal Blending Organic Corrosion Inhibitor for Carbon Steel in Chloride Contaminated Simulated Concrete Pore Solution, *J. Adv. Concr. Technol*., 2020, **18**, no. 3, 116–128. doi: 10.3151/jact.18.116
24. K. Amgain, B.N. Subedi, S. Joshi and J. Bhattarai, A Comparative Study of the Anticorrosive Response of *Tinospora cordifolia* Stem Extract for Al and Cu in Biodiesel-based Fuels, *E3S Web Conf*., 2022, **355**, 01005. doi: 10.1051/e3sconf/202235501005
25. L. Alvarez, O.T. de Rincón, J. Escribano and B.R. Troconis, Organic Compounds as Corrosion Inhibitors for Reinforced Concrete: A Review, *Corros. Rev*., 2023, **41**, no. 6, 617–634. doi: 10.1515/corrrev-2023-0017
26. N.O. Eddy, A.O. Odiongenyi, E.E. Ebenso, R. Garg and R. Garg, Plant Wastes as Alternative Sources of Sustainable and Green Corrosion Inhibitors in Different Environments, *Corros. Eng. Sci. Technol*., 2023, **58**, no. 5, 521–533. doi: 10.1080/1478422X.2023.2204260
27. S.A. Umoren, M.M. Solomon, I.B. Obot and R.K. Suleiman, A Critical Review on the Recent Studies on Plant Biomaterials as Corrosion Inhibitors for Industrial Metals, *J. Ind. Eng. Chem*., 2019, **76**, 91–115. doi: 10.1016/j.jiec.2019.03.057
28. A. Giri, M. Gautam, A. Roka, N.P. Bhattarai and J. Bhattarai, Performance of anticorrosive measures of steel in concrete infrastructure by plant-based extracts, *Macromol. Symp*., 2023, **410**, no. 1, 2200115. doi: 10.1002/masy.202200115
29. U.M. Angst, Challenges and Opportunities in Corrosion of Steel in Concrete, *Mater. Struct*., 2018, **51**, 4. doi: 10.1617/s11527-017-1131-6
30. E.S.J. Ahmed and G.M. Ganesh, A Comprehensive Overview on Corrosion in RCC and Its Prevention Using Various Green Corrosion Inhibitors, *Buildings*, 2022, **12**, no. 10, 1682. doi: 10.3390/buildings12101682
31. S. Ghoreishiamiri, P.B. Raja, M. Ismail, S.F.H. Karouei and P. Forouzani, *Areca catechu*: An Eco-friendly Corrosion Inhibitor for Reinforced Concrete Structures in Corrosive Medium, *J. Bio Tribo Corros*., 2021, **7**, 22. doi: 10.1007/s40735-020-00464-6
32. B. Valdez-Salas, R. Vazquez-Delgado, J. Salvador-Carlos, E. Beltran-Partida, R. Salinas-Martinez, N. Cheng and M. Curiel-Alvarez, *Azadirachta indica* Leaf Extract as Green Corrosion Inhibitor for Reinforced Concrete Structures: Corrosion Effectiveness Against Commercial Corrosion Inhibitors and Concrete Integrity, *Materials*, 2021, **14**, no. 12, 3326. doi: 10.3390/ma14123326
33. M. Rana, S. Joshi and J. Bhattarai, Extract of Different Plants of Nepalese Origin as Green Corrosion Inhibitor for Mild Steel in 0.5 M NaCl Solution, *Asian J. Chem*., 2017, **29**, no. 5, 1130–1134. doi: 10.14233/ajchem.2017.20449

34. Q. Wang, X. Wu, H. Zheng, L. Liu, Q. Zhang, A. Zhang, Z. Yan, Y. Sun, Z. Li and X. Li, Evaluation for *Fatsia japonica* Leaves Extract (FJLE) as Green Corrosion Inhibitor for Carbon Steel in Simulated Concrete Pore Solutions, *J. Build. Eng*., 2023, **63**, 105568. doi: 10.1016/j.jobe.2022.105568
35. R. Naderi, A. Bautista, F. Velasco, M. Soleimani and M. Pourfath, Green Corrosion Inhibition for Carbon Steel Reinforcement in Chloride-polluted Simulated Concrete Pore Solution Using *Urtica dioica* Extract, *J. Build. Eng*., 2022, **58**, 105055. doi: 10.1016/j.jobe.2022.105055
36. Q. Liu, Z. Song, H. Han, S. Donkor, L. Jiang, W. Wang and H. Chu, A Novel Green Reinforcement Corrosion Inhibitor Extracted from Waste *Platanus acerifolia* Leaves, *Constr. Build. Mater*., 2020, **260**, 119695. doi: 10.1016/j.conbuildmat.2020.119695
37. M.T. Madanan, I.K. Shah, G.K. Varghese and R.K. Kaushal, Application of Aztec Marigold (*Tagetes erecta L*.) for Phytoremediation of Heavy Metal Polluted Lateritic Soil, *Environ. Chem. Ecotoxicol*., 2021, **3**, 17–22. doi: 10.1016/j.enceco.2020.10.007
38. A. Kambhu, T. Satapanajaru, P. Somsamak, P. Pengthamkeerati, C. Chokejaroenrat, K. Muangkaew and K. Nonthamit, Green Cleanup of Styrene-contaminated Soil by Carbon-based Nanoscale Zero-valent Iron and Phytoremediation: Sunn Hemp (*Crotalaria juncea*), Zinnia (*Zinnia violacea* Cav.), and Marigold (*Tagetes erecta* L.), *Heliyon*, 2024, **10**, no. 6, e27499. doi: 10.1016/j.heliyon.2024.e27499
39. Z. Li and J. Peng, Raman Spectroscopy and Electrochemical Analysis of the Corrosion Behaviour of Reinforcing Steel in the Presence of TEE as an Inhibitor, *Int. J. Electrochem. Sci*., 2017, **12**, no. 9, 8177–8187. doi: 10.20964/2017.09.52
40. P. Mourya, S. Banerjee and M.M. Singh, Corrosion Inhibition of Mild Steel in Acidic Solution by *Tagetes erecta* (Marigold Flower) Extract as a Green Inhibitor, *Corros. Sci*., 2014, **85**, 352−363. doi: 10.1016/j.corsci.2014.04.036
41. N. Hossain, M.A. Islam and M.A. Chowdhury, Advances of Plant-extracted Inhibitors in Metal Corrosion Reduction - Future Prospects and Challenges, *Results Chem*., 2023, **5**, 100883. doi: 10.1016/j.rechem.2023.100883
42. S. Yadav, G. Choudhary and A. Sharma, Green Approach to Corrosion Inhibition of Aluminum and Copper by *Ziziphus mauritiana* Fruit Extract in Hydrochloric Acid Solution, *Int. J. ChemTech Res*., 2013, **5**, no. 4, 1815–1823.
43. K.R. Bhattarai and M.L. Pathak, A New Species of Ziziphus (*Rhamnaceae*) from Nepal Himalayas, *Indian J. Plant Sci*., 2015, **4**, no. 2, 71−77.
44. B.N. Subedi, K. Amgain, S. Joshi and J. Bhattarai, Green Approach to Corrosion Inhibition Effect of *Vitex negundo* Leaf Extract on Aluminum and Copper Metals in Biodiesel and Its Blend, *Int. J. Corros. Scale Inhib*., 2019, **8**, no. 3, 744−759. doi: 10.17675/2305-6894-2019-8-3-21
45. J. Bhattarai, M. Rana, M.R. Bhattarai and S. Joshi, Effect of Green Corrosion Inhibitor of Callistemon Plant Extract on the Corrosion Behavior of Mild Steel in NaCl and HCl Solutions, *Corcon 2016, Publication of NIGIS/NACE*, 2016, MI-17.

46. J. Bhattarai, Passivation Behavior of Steel Rod and Wires of Nepal in Acidic and Alkaline Solutions, *Nepal J. Sci. Technol*., 2008, **9**, 157–162. doi: 10.3126/njst.v9i0.3181
47. P. Magrati, D.B. Subedi, D.B. Pokharel and J. Bhattarai, Appraisal of Different Inorganic Inhibitors Action on the Corrosion Control Mechanism of Mild Steel in HNO_3 Solution, *J. Nepal Chem. Soc*., 2020, **41**, no. 1, 64–73. doi: 10.3126/jncs.v41i1.30489
48. Y.I. Kuznetsov, N.N. Andreev and S.S. Vesely, Why We Reject Papers with Calculations of Inhibitor Adsorption Based on Data on Protective Effects, *Int. J. Corros. Scale Inhib*., 2015, **4**, 108–109. doi: 10.17675/2305-6894-2015-4-1-108-109
49. K. Amgain, B.N. Subedi, S. Joshi and J. Bhattarai, Investigation on the Effect of *Tinospora cordifolia* Plant Extract as a Green Corrosion Inhibitor to Aluminum and Copper in Biodiesel and its Blend, *Corcon 2018, Publication of NIGIS/NACE*, 2018, PP19.
50. G. Song, Theoretical Analysis of the Measurement of Polarization Resistance in Reinforced Concrete, *Cem. Concr. Compos*., 2000, **22**, no. 6, 407–415. 10.1016/S0958-9465(00)00040-8
51. C.L. Reedy, R.A. Corbett and M. Burke, Electrochemical Tests as Alternatives to Current Methods for Assessing Effects of Exhibition Materials on Metal Artifacts, *Stud. Conserv*., 1998, **43**, 183–196. doi: 10.2307/1506745
52. A.S. Fouda, A.M. El-desoky and D.M. Ead, Anhydride Derivatives as Corrosion Inhibitors for Carbon Steel in Hydrochloric Acid Solutions, *Int. J. Electrochem. Sci*., 2013, **8**, 8823–8847.
53. I. Langmuir, The Constitution and Fundamental properties of Solids and Liquids: part I-Solid, *J. Am. Chem. Soc*., 1916, **38**, no. 11, 2221–2295. doi: 10.1021/ja02268a002
54. M.I. Temkin, Adsorption Equilibrium and the Kinetics of Processes on Non-homogeneous Surfaces and in the Interaction Between Adsorbed Molecules, *Zhurnal Fizicheskoi Khimii*, 1941, **15**, 296–332 (in Russian).
55. M. Gautam, D.B. Subedi, J. Dhungana, N.P. Bhattarai and J. Bhattarai, Utilization of Bark Extract of *Phyllanthus emblica* as a Sustainable Corrosion Inhibitor to Reinforced Concrete Infrastructures in Aggressive Environments, *E3S Web Conf*., 2024, in press.
56. M. Elaloui, A. Laamouri, A. Ennajah, M. Cerny, C. Mathieu, G. Vilarem, H. Chaar and B. Hasnaoui, Phytoconstituents of Leaf Extracts of *Ziziphus jujuba* Mill. Plants Harvested in Tunisia, *Ind. Crops. Prod*., 2016, **83**, 133–139. doi: 10.1016/j.indcrop.2015.11.029
57. E. El Maaiden, Y. El Kharrassi, N.A.S. Qarah, A.K. Essamadi, K. Moustaid, and B. Nasser, Genus Ziziphus: A Comprehensive Review on Ethnopharmacological, Phytochemical and Pharmacological Properties, *J. Ethnopharm*., 2020, **259**, 112950. doi: 10.1016/j.jep.2020.112950
58. D. Chaudhari, A. Muthal, A. Mali, M. Salunke and V. Shinde, Phytochemical and Pharmacological Activities of *Tagetes erecta* L: An Updated Review, *Int. J. Herb. Med*., 2024, **12**, no. 1, 10–15. doi: 10.22271/flora.2024.v12.i1a.915

59. P.H. Chaudhary, Pharmacognostical and Phytochemical Studies on Leaves of *Tagetes erecta* Linn, *J. Ayurveda Integ. Med. Sci*., 2023, **8**, no. 7, 29–36. doi: 10.21760/jaims.8.7.5
60. A. Sulistiawan, W. Setyaningsih and A. Rohman, A New FTIR Method Combined with Multivariate Data Analysis for Determining Aflatoxins in Peanuts (*Arachis hypogaea*), *J. Appl. Pharm. Sci*., 2022, **12**, 199–206. doi: 10.7324/JAPS.2022.120720
61. E. Saifitri, H. Humaira, N. Nazaruddin, S. Susilawati, M. Murniana and N.D. Md Sani, *Dioscorea alata* L. Anthocyanin Extract as Methanol as a Sensitive pH Active Compound, *J. Phys.: Conf. Ser*., 2021, **1869**, no. 1, 012508. doi: 10.1088/1742-6596/1869/1/012058
62. P.P. Yue, Y.J. Hu, G.Q. Fu, C.X. Sun, M.F. Li, F. Peng and R.C. Sun, Structural Differences Between the Lignin-Carbohydrate Complexes (LCCs) from 2- and 24-Month-Old Bamboo (*Neosinocalamus affinis*), *Int. J. Mol. Sci*., 2018, **19**, no. 1, 1. doi: 10.3390/ijms19010001
63. J.M. Barcelo, A.M. Gatchallan, I.J.B. Aquino, D.R.E. Ollero, F.I.D. Cortez, T.M. Costales and L.A.Q. Marzo, FTIR Spectrum and Antimutagenicity of *Coffea arabica* Pulp and *Arachis hypogaea* Test in Relation to Their *in vitro* Antioxidant Properties, *Asia Pac. J. Multidiscip. Res*., 2015, **3**, no. 4, 99–108.
64. K.K. Veedu, T.P. Kalarikkal, N. Jayakumar and N.K. Gopalan, Anticorrosive Performance of *Mangifera indica* L. leaf Extract-based Hybrid Coating on Steel, *ACS Omega*, 2019, **4**, no. 6, 10176–10184. doi: 10.1021/acsomega.9b00632
65. H. Long, L. Chen, B. Dong, Y. Sun, Y. Yan and C. Chen, The Electronic Properties and Surface Chemistry of Passive Film on Reinforcement: Effect of Composition of Simulated Concrete Pore Solution, *Const. Buil. Mater*., 2022, **360**, 129567. doi: 10.1016/j.conbuildmat.2022.129567
66. N. Pandey, L. Gupta, M. Gautam, J. Bhattarai and N.P. Bhattarai, An Inhibitory Prospect of Leaf Extracts of Flossflower and Yam for Rebar Steel Corrosion in Concrete Aggregates, *E3S Web Conf*., 2024, **559**, 02008. doi: 10.1051/e3sconf/202455902008
67. H. Lgaz and H.S. Lee, Interfacial Adsorption Mechanism of Hydroxycinnamic Acids on Iron Surfaces: A Computational Perspective Toward Eco-friendly Corrosion Mitigation Strategies, *Appl. Surf. Sci*., 2024, **644**, 158763. doi: 10.1016/j.apsusc.2023.158763
68. G. Venkatesh, C. Kamal, P. Vennila, S. Kaya, M.G.L. Annaamalai and B.E. Ibrahimi, Sustainable Corrosion Inhibitor for Steel Embedded in Concrete by Guar Gum: Electrochemical and Theoretical Analyses, *Appl. Surf. Sci. Adv*., 2022, **12**, 100328. doi: 10.1016/j.apsadv.2022.100328
69. M. Tempkin and V. Pyzhev, Kinetics of the Synthesis of Ammonia on Promoted Iron Catalysts, *Acta Physicochim. URSS*, 1940, **12**, no. 1, 217–222.
70. C.C. Ahanotu, I.B. Onyeachu, M.M. Solomon, I.S. Chikwe, O.B. Chikwe and C.A. Eziukwu, *Pterocarpus santalinoides* Leave Extract as a Sustainable and Potent Inhibitor for Low Carbon Steel in a Simulated Pickling Medium, *Sustainable Chem. Pharm*., 2020, **15**, 100196. doi: 10.1016/j.scp.2019.100196

71. T.H. Tran, A.H. Le, T.H. Pham, D.T. Nguyen, S.W. Chang, W.J. Chung and D.D. Nguyen, Adsorption Isotherms and Kinetic Modeling of Methylene Blue Dye onto a Carbonaceous Hydrochar Adsorbent Derived from Coffee Husk Waste, *Sci. Total Environ.*, 2020, **725**, 138325. doi: 10.1016/j.scitotenv.2020.138325
72. M.T. Amin, A.A. Alazba and M. Shafiq, Adsorptive Removal of Reactive Black 5 from Wastewater Using Bentonite Clay: Isotherms, Kinetics and Thermodynamics, *Sustainability*, 2015, **7**, 15302−15318. doi: 10.3390/su71115302
73. P. Katuwal, R. Regmi, S. Joshi and J. Bhattarai, Assessment on the Effective Green-Based Nepal Origin Plants Extract as Corrosion Inhibitor for Mild Steel in Bioethanol and its Blend, *European Journal of Advanced Chemistry Research*., 2020, **1**, no. 5. doi: 10.24018/ejchem.2020.1.5.16
74. A. Hashem, C.O. Aniagor, S. Farag, M. Fikry, A.A. Aly and A. Amr, Evaluation of the Adsorption Capacity of Surfactant-modified Biomass in an Aqueous Acid Blue 193 System, *Waste Management Bulletin*, 2024, **2**, no. 1, 172–183. doi: 10.1016/j.wmb.2024.01.004
75. O.F. Akinyele, A.S. Adekunle, A.A. Akinmuyisitan, S.S. Durodola, O.E. Oyeneyin, N.D. Ojo and L. O. Olasunkanmi, Adsorption, Synergistic Inhibitive Potentials and Quantum Chemical Studies of (E)-1-(2-((2,4-dimethoxyphenyl)diazenyl)Phenyl)-2-Hydroxy-2-Phenylethan-1-one as Mild Steel Anticorrosion Agent in Acidic Medium, *Results Surf. Interf*., 2023, **12**, 100128. doi: 10.1016/j.rsurfi.2023.100128
76. U. Mamudu, M.S. Alnarabiji and R.C. Lim, Adsorption Isotherm and Molecular Modeling of phytoconstituents from *Dillenia suffruticosa* Leaves for Corrosion Inhibition of Mild Steel in 1.0 M Hydrochloric Acid Solution, *Results Surf. Interf*., 2023, **13**, 100145. doi: 10.1016/j.rsurfi.2023.100145
77. D.B. Subedi, D. B. Pokharel and J. Bhattarai, Assessment on the Effects of Sodium Salts of Tungstate and Nitrite as Green Inhibitor for the Corrosion of Cr–5Ni–53W Alloy in 0.5 M NaCl Solution, *Int. J. Metallurgy Alloys*, 2020, **6**, no. 1, 25−36.
78. L. Popoola, Organic Green Corrosion Inhibitors (OGCIs): A Critical Review, *Corros. Rev*., 2019, **37**, no. 2, 71−102. doi: 10.1515/corrrev-2018-0058
79. C.A. Maduabuchi, D.I. Njoku, O.I. Anthony, S.C. Nwanonenyi, C. Akalezi, A. Blessing and E.E. Oguzie, Experimental and Theoretical Studies on the Protective Effect of a Biomass Corrosion Inhibitor (*Vigna radiata*) on Mild Steel in Acidic Medium, *Electroanalysis*, 2020, **32**, 3117−3130. doi: 10.1002/elan.202060378
80. N. Bhardwaj, P. Sharma and V. Kumar, Phytochemicals as Steel Corrosion Inhibitor: An Insight into Mechanism, *Corros. Rev*., 2021, **39**, no. 1, 27−41. doi: 10.1515/corrrev-2020-0046
81. F. Kaya, R. Solmaz and I.H. Gecibesler, The Use of Methanol Extract of *Rheum Ribes* (Isgın) Flower as a Natural and Promising Corrosion Inhibitor for Mild Steel Protection in 1 M HCl Solution, *J. Ind. Eng. Chem*., 2023, **122**, 102–117. doi: 10.1016/j.jiec.2023.02.013

82. A.R. Sayed, M.M. Saleh, M.A. Al-Omair, H.M. Abd Al-Lateef, Efficient Route Synthesis of New Polythiazoles and Their Inhibition Characteristics of Mild-steel Corrosion in Acidic Chloride Medium, *J. Mol. Struck*., 2019, **1184**, 452–461. doi: 10.1016/j.molstruc.2019.02.061
83. E. Alibakhshi, M. Ramezanzadeh, S.A. Haddadi, G. Bahlakeh, B. Ramezanzadeh and M. Mahdavian, Persian liquorice Extract as a Highly Efficient Sustainable Corrosion Inhibitor for Mild Steel in Sodium Chloride Solution, *J. Cleaner Prod*., 2019, **210**, 660−672. doi: 10.1016/j.jclepro.2018.11.053
84. A. Bahir, B. Imen and N. Alqarni, Advancing Imine Metal Chelates for Corrosion Inhibition Across Diverse Environments: A Novel Perspective, *Results Chem*., 2024, **7**, 101455. doi: 10.1016/j.rechem.2024.101455
85. C. Sun, M. Sun, J. Liu, Z. Dong, L. Fan and J. Duan, Anti-Corrosion Performance of Migratory Corrosion Inhibitors on Reinforced Concrete Exposed to Varying Degrees of Chloride Erosion, *Materials*, 2022, **15**, no. 15, 5138. doi: 10.3390/ma15155138
86. V. Grudić, I. Boskovic, S. Martinez and B. Knezevic, Study of Corrosion Inhibition for Mild Steel in NaCl Solution by Propolis Extract, *Macedonian J. Chem. Chem. Eng*., 2018, **37**, no. 2, 203−213. doi: 10.20450/mjcce.2018.1513
87. Y. Idell, B. Au, A. Jaycox, W. Siekhaus, C. Saw, K. Blobaum and W. McLean, White-light Interferometry for Early-stage Metal Oxide Growth Characterization, *Meas. Sci. Technol*., 2020, **31**, no. 10, 105201. doi: 10.1088/1361-6501/ab9129
88. C.K. Tao, Y.J. Wu, W.Y. Wang, Y.S. Qian, R. Tao and T. Kang, Experimental Investigation of White-Light Interferometry Based on Sub-dark-field Illumination, *Opt. Commun*., 2019, **435**, 108–117. doi: 10.1016/j.optcom.2018.11.020
89. Z. Zhang and J. Su, Simulation and Reconstruction of 3D Microscopic Morphology of Damaged Optical Film Surface, *Acta Opt. Sin*., 2021, **41**, no. 2, 0212002. doi: 10.3788/AOS202141.0212002
90. B. Holme and O. Lunder, Characterisation of Pitting Corrosion by White Light Interferometry, *Corros. Sci*., 2007, **49**, no. 2, 391−401. doi: 10.1016/j.corsci.2006.04.022
91. A. Sidiq, S. Setunge, P.K. Annamalai, R.J. Gravina and F. Giustozzi, Concrete Self-healing Performance Using Surface Roughness Parameters: Metrological Approach, *J. Build. Eng*., 2024, **90**, 109433. doi: 10.1016/j.jobe.2024.109433
92. X. Zhao, Y. Cui, H. Wei, X. Kong, P. Zhang and C. Sun, Research on Corrosion Detection for Steel Reinforced Concrete Structures Using the Fiber Optical White Light Interferometer Sensing Technique, *Smart Mater. Struct*., 2013, **22**, no. 6, 065014. doi: 10.1088/0964-1726/22/6/065014

♦ ♦ ♦